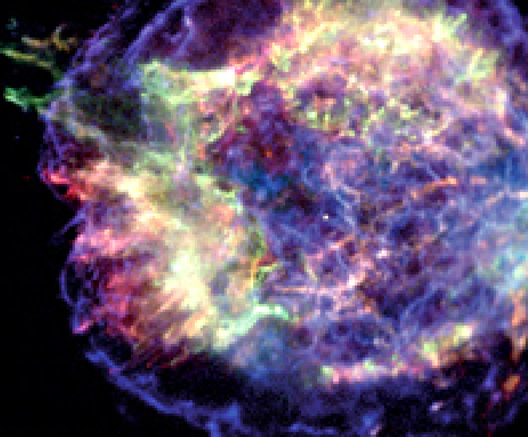

Second Edition

Exploring the X-ray Universe

Frederick D. Seward and Philip A. Charles

CAMBRIDGE

CAMBRIDGE www.cambridge.org/9780521884839

This page intentionally left blank

Exploring the X-ray Universe

Second Edition

Capturing the excitement and accomplishments of X-ray astronomy, this second edition now includes a broader range of astronomical phenomena and dramatic new results from the most powerful X-ray telescopes.

Covering all areas of astronomical research, ranging from the smallest to the largest objects, from neutron stars to clusters of galaxies, this textbook is ideal for undergraduate students and will appeal to amateur astronomers and scientists with a general interest in astronomy. Each chapter starts with the basic aspects of the topic, explores the history of discoveries, and examines in detail modern observations and their significance. This new edition has been updated with 15 years of observations from recent space-based instruments, including results from the Hubble Space Telescope, ASCA, RossiXTE, BeppoSAX, Chandra, XMM–Newton and Swift. New chapters cover X-ray emission processes, the Interstellar Medium, the Solar System, and gamma-ray bursts. The text is supported by more than 300 figures, with tables listing the properties of the sources, and more specialised technical points separated in boxes.

Frederick D. Seward has been leader of the High Altitude Physics Group at the Lawrence Livermore Laboratory, Director of the Einstein Guest Observer Program at the Harvard-Smithsonian Center for Astrophysics, Head of Chandra User Support and an Assistant Director of the Chandra Observatory before retiring in 2004.

Philip A. Charles is Director of the South African Astronomical Observatory, which operates SALT, the largest telescope in the Southern Hemisphere. He has recently been Head of the Astronomy Group at the University of Southampton's School of Physics and Astronomy.

Exploring the X-ray Universe

Second Edition

Frederick D. Seward
Harvard-Smithsonian Center for Astrophysics

Philip A. Charles
South African Astronomical Observatory

CAMBRIDGE
UNIVERSITY PRESS

CAMBRIDGE UNIVERSITY PRESS
Cambridge, New York, Melbourne, Madrid, Cape Town, Singapore,
São Paulo, Delhi, Dubai, Tokyo

Cambridge University Press
The Edinburgh Building, Cambridge CB2 8RU, UK

Published in the United States of America by Cambridge University Press, New York

www.cambridge.org
Information on this title: www.cambridge.org/9780521884839

First published in print format 2010

ISBN-13 978-0-511-77150-7 eBook (Adobe Reader)

ISBN-13 978-0-521-88483-9 Hardback

Contents

The colour plates will be found between pages 312 and 313.

List of acronyms

AAT	Anglo-Australian Telescope
AAVSO	American Association of Variable Star Observers
ACIS	Advanced CCD Imaging Spectrometer
AGN	Active Galactic Nuclei
ANS	Astronomische Nederlandse Satelliet
ASCA	Advanced Satellite for Cosmology & Astrophysics
AS&E	American Science & Engineering
ASM	All-Sky Monitor
AU	Astronomical Unit
AXAF	Advanced X-ray Astrophysics Facility
AXP	Anomalous X-ray Pulsar
BATSE	Burst and Transient Source Experiment
BBSO	Big Bear Solar Observatory
CAL	Columbia Astrophysics Laboratory
CCD	Charge-Coupled Device
CCO	Central Compact Object
CD	Contact Discontinuity
CfA	Center for Astrophysics
CGRO	Compton Gamma-Ray Observatory
CMB	Cosmic Microwave Background
CT	Charge Transfer
CV	Cataclysmic Variable
CXC	Chandra X-ray Center
CXO	Chandra X-ray Observatory
DEM	Differential Emission Measure
DIM	Disc-Instability Model
DSS	Digital Sky Survey
DXS	Diffuse X-ray Spectrometer
EM	Emission Measure
EPIC	European Photon Imaging Camera
ESA	European Space Agency
EUVE	Extreme Ultraviolet Explorer
EXOSAT	European X-ray Observatory Satellite
FIR	Far Infrared
FPCS	Focal Plane Crystal Spectrometer
FS	Forward Shock
FWHM	Full-Width at Half Maximum
GGS	Global Geospace Science
GIS	Gas Imaging Spectrometer
GRB	Gamma-ray Burst
GSFC	Goddard Space Flight Center
GSPC	Gas-scintillation Proportional Counter
HDF	Hubble Deep Field
HEASARC	High Energy Astrophysics Science Archive Research Center (at NASA's GSFC)

HEAO	High Energy Astronomy Observatory
HETE	High Energy Transient Explorer
HETG	High Energy Transmission Grating
HEXTE	High Energy X-ray Timing Experiment
HMXB	High-Mass X-ray Binary
HR	Hertzsprung-Russell
HRC	High Resolution Camera
HRI	High Resolution Imager
HST	Hubble Space Telescope
IBIS	Imager on Board INTEGRAL Satellite
ICM	Intracluster Medium
IMBH	Intermediate-Mass Black Hole
INTEGRAL	International Gamma-Ray Astrophysics Laboratory
IP	Intermediate Polar
IPC	Imaging Proportional Counter
IPN	Interplanetary Network
IR	Infrared
ISAS	Institute of Space and Astronautical Science
ISM	Interstellar Medium
IUE	International Ultraviolet Explorer
JAXA	Japan Aerospace Exploration Agency
LANL	Los Alamos National Laboratory
LBA	Long Baseline Array
LBV	Luminous Blue Variable
LE	Low Energy
LETGS	Low Energy Transmission Grating Spectrometer
LHB	Local Hot Bubble
LINEAR	Lincoln Near-Earth Asteroid Research project
LLL	Lawrence Livermore Laboratory
LMC	Large Magellanic Cloud
LMMSC	Lockheed Martin Missiles and Space Company
LMXB	Low-Mass X-ray Binary
MCV	Magnetic Cataclysmic Variable
MCP	Micro Channel Plate
ME	Medium Energy
MIT	Massachusetts Institute of Technology
MG	MegaGauss
MOS	Metal Oxide Semiconductor
MPC	Monitor Proportional Counter
MPE	Max-Plank-Institut für Extraterrestrisch Physik
MSFC	Marshall Space Flight Center
NASA	National Aeronautics and Space Administration
NAOJ	National Astronomical Observatory of Japan
NGC	New General Catalog
NGST	Northrop-Grumman Space Technology
NIST	National Institute of Standards and Technology
NJIT	New Jersey Institute of Technology
NOAA	National Oceanic and Atmospheric Administration
NRL	Naval Research Laboratory

OGS	Objective Grating Spectrometer
OM	Optical Monitor
OSO	Orbiting Solar Observatory
PCA	Proportional Counter Array
PIXIE	Polar Ionospheric X-ray Imaging Experiment
PMS	Pre-Main Sequence
PSF	Point Spread Function
PSPC	Position-Sensitive Proportional Counter
PSR	Pulsar
PWN	Pulsar Wind Nebula
QPO	Quasi-Periodic Oscillation
QSO	Quasistellar Object
RASS	ROSAT All-Sky Survey
RGS	Reflection Grating Spectrometer
ROSAT	ROentgen SATellit
R-T	Rayleigh-Taylor
RXTE	Rossi X-ray Timing Explorer
SAAO	South African Astronomical Observatory
SAS	Small Astronomy Satellite
SAO	Smithsonian Astrophysical Observatory
SGR	Soft Gamma-ray Repeater
SIS	Solid-state Imaging Spectrometer
SMC	Small Magellanic Cloud
SN	Supernova
SNR	Supernova Remnant
SSL	Space Sciences Laboratory
SSS	Solid-State Spectrometer
SSS	Supersoft Source
STFC	Science & Technology Facilities Council
STScI	Space Telescope Science Institute
SWPC	Space Weather Prediction Center
TOO	Target of opportunity
ULX	Ultra-Luminous X-ray source
UV	Ultraviolet
UT	Universal Time
VLA	Very Large Array
WFC	Wide Field Camera
WC	Wolf-Rayet (carbon-rich)
WR	Wolf-Rayet
XLF	X-ray Luminosity function
XMM	X-ray Multi-Mirror Mission
XRO	X-ray Outburst
XRB	X-ray Binary
XRT	X-ray Telescope
ZAMS	Zero Age Main Sequence

Foreword

This is a book about X-ray astronomy. We take a historical perspective because this is how we saw it happen and because this gives a feeling for the observable universe. In a table listing all members of a class of objects, the brightest source does not stand out, but in the first observation, it is a splendid object and remembered fondly by those involved in the discovery.

Some 50 years ago X-rays from stars other than our Sun were unknown and unexpected by all but a few pioneering scientists. Since the discovery of cosmic X-rays in 1962 the field has grown at an astonishing rate. Since the first edition of this book, published in 1995 and including results from the first X-ray telescopes, the sensitivity of X-ray observations has increased dramatically. In 1999 the Chandra and XMM X-ray observatories were launched and, in 10 years of operation, have produced X-ray images of comparable angular resolution to those obtained by the largest ground-based observatories. More importantly, X-ray spectroscopy of sufficient resolution to allow comparison with spectra at other wavelengths has become possible. Technical improvements in dispersive spectroscopy mean that high resolution X-ray spectra of faint sources have become available for the first time. This has helped propel X-ray astronomy to its rightful place as a sub-discipline of astronomy, where a knowledge of truly multiwavelength results is necessary for the study of any class of objects. This book, however, is about X-rays. Observations at other wavelengths are sometimes included but space limitations mean that thorough coverage is beyond the scope of the book, although we try to give suitable references and links.

We are observers, so, although this book is primarily about the science of X-ray sources, there are excursions into instrumentation and techniques. Our research has been mostly galactic, as all the bright X-ray sources are nearby and have been available for study from the earliest days of this field. This means that there is somewhat less detail in chapters concerning sources at much greater distances, but our understanding of the early universe and cosmology is developing rapidly at the present time. We have each written chapters concerning our respective special interests but could not cover all aspects. We were trained in nuclear physics (FDS) and optical/X-ray astronomy (PAC). These backgrounds probably shine through in some of the material covered. We hope all major areas touched by X-ray astronomy are included.

The material is written for someone with an astronomical background, but each chapter starts simply so those with no background can understand the basics. For people who do not wish to read all the details, we have separated some technical discussions into boxes that accompany the text. An acquaintance with physics and mathematics is helpful in understanding some of the boxed material but the main text is presented so that it can be followed without the boxes.

Most of the illustrations have already appeared in the scientific literature. A few are from our own work and we thank our colleagues who have generously given material generated by their research. Although many references have been added, we have not given extensive accreditation in order to make the text more readable (and not outrageously long). The bibliography for each chapter includes some popular articles and scientific reviews. Material obtained from the Internet is referenced by the Internet address (URL) and sometimes by a more-descriptive publication.

Some scientists who have made key observations or developed key theories are mentioned in the text but many are not. We apologise to our friends and colleagues for the omissions. We also recognise that astronomers only contribute part of the effort necessary for a successful space astronomy mission. There is planning, funding, building, calibration, launch, control during observations, data transmission and collection, and the data must be made available to observers in an understandable format. The scientific process also includes editors, referees, and those who evaluate proposals. X-ray astronomy now is very much a group effort, a national or international effort for the large missions. Our colleagues at NASA and ESA are career scientists who manage ongoing programs, administer the funding, and plan the future of X-ray astronomy. This is a difficult and, at times, a thankless job. Successful proposers think winning is their just due. Unsuccessful proposers think the process is flawed. It is easier to make enemies than friends. We wish them adequate funding and success with future projects.

We would like to thank those who took the trouble to contact us with comments about and corrections to our 1st edition, for which we are very grateful. We also thank our many colleagues and friends for providing us with material, particularly diagrams, that we have included in this new edition. In particular, we appreciate helpful discussions with Jeremy Drake, Bill Forman, Dave Huenemoerder, Dong-Woo Kim, Andrea Prestwich, John Raymond, Pat Slane, Jan Vrtilek, and Scott Wolk. We hope their input has been fairly treated.

We, the authors, have been observers of celestial X-rays since 1965 (FDS) and 1972 (PAC). We miss the early days when a person could easily name from memory all the known X-ray sources and when the nature of many were unknown. There are now so many instruments and sources that we are challenged to even list the observatories or categories of objects. Many of the major discoveries have been serendipitous in nature, leading to an exciting, but at times chaotic, growth in the field (a process reflected perhaps across all of observational science). We have nevertheless organised the material and note with satisfaction that the underlying physical mechanism of most cosmic sources is now, at some level, understood. We hope that you gain knowledge and enjoyment from this book.

Phil Charles – South African Astronomical Observatory
Fred Seward – Smithsonian Astrophysical Observatory

Chapter 1

Birth and childhood of X-ray astronomy

1.1 The discovery of X-rays

On the second story of the building at Röntenring 8 in Würzburg, Germany, there is a plaque: 'In diesem Hause entdekte W. C. Röntgen im Jahre 1895 die nach ihm benannten Strahlen' – In this building, in the year 1895, W. C. Röntgen discovered the radiation named for him. Here was the laboratory of Wilhelm C. Röntgen, a 50-year-old professor of physics, who was studying phenomena associated with electrical discharge in gasses. On the afternoon of 8 November, working alone in his laboratory, he noticed a curious phenomenon. When high voltage was applied to the electrodes in the partially evacuated glass discharge tube, he noticed a faint glow from a fluorescent screen placed at the other end of the laboratory table. The room was dark and he had previously covered the tube with black cardboard so no light would escape. Why was the screen glowing?

That evening he verified that the discharge tube was indeed the source of the energy that caused the screen to glow, and that no visible radiation was escaping from the shrouded tube. He quickly found that the unknown radiation would pass through paper, wood, and aluminum but was stopped by heavy metals. Then, when holding a lead disc in front of the screen to observe its shadow, Röntgen also saw the shadow of bones in his hand! In a week he had measured the basic characteristics of this new form of radiation. He persuaded his wife, Bertha, to hold her hand steadily over a photographic plate for 15 minutes, making a picture showing hand and finger bones as grey shadows and the shadow of her ring sharp and black. He sent this picture and a description of his results to be published and to other scientists. He called these new rays 'X-rays' but others called them 'Röntgenstrahlung' – Röntgen radiation. The medical applications were immediately obvious and commercial X-ray machines were soon available.

The discovery of X-rays is one of the most famous serendipitous discoveries of science (Colour Plate 4). If Röntgen had been funded to investigate ways to help doctors in hospitals set broken bones, it is unlikely that he would have pursued this line of research.

In 1901, Röntgen was awarded the first Nobel Prize in physics. In 1990, a German satellite devoted to X-ray astronomy was placed in orbit and operated for 10 years. The satellite was named ROSAT (for Röntgen Satellite) and was taking data on the 100th anniversary of Röntgen's discovery. In 2002, Riccardo Giacconi was awarded the Nobel Prize in physics for pioneering work in X-ray astronomy. The authors of this book have had the pleasure of knowing Riccardo and, years ago, of observing the source he discovered, Sco X-1. Now, 115 years after Röntgen's discovery, we are finishing the initial period of exploration, and X-ray astronomy has become part of the general field of astronomy. Like traditional optical astronomers, we work with telescopes that record hundreds of sources in each field. It is still fun.

1.2 Properties of X-rays

We know now that X-rays are a form of electromagnetic radiation, like visible light, but the individual quanta of radiation, the photons, have energies a thousand times that of optical photons. Visible light, in general, does not penetrate matter. The photons are scattered from or absorbed at the surface of opaque objects. Visible light will also pass through transparent substances and will reflect from smooth surfaces. X-rays, on the other hand, go right through the surfaces of all substances. The individual photons, traveling in straight lines, either interact with individual atoms or pass through unaffected. The probability of interaction increases with Z, the atomic number of the element. Thus, in Röntgen's picture of Bertha's hand, the X-rays passed easily through the carbon ($Z = 6$) and oxygen ($Z = 8$) of flesh, but many photons were absorbed by the calcium ($Z = 20$) of bones, and all were absorbed by the gold ($Z = 79$) ring that was on her finger. The probability of interaction also depends on photon energy. More energetic photons are less likely to be absorbed.

X-rays are usually generated by accelerating an electron beam with high voltage and directing the beam to strike a tungsten target. The energy of the X-ray photons is measured in kilo-electron volts (keV), the voltage used to accelerate the electrons. A potential of 100 000 volts, for example, is capable of producing 100 keV X-rays.

1.3 The difficulties of observing X-rays from stars

Röntgen's X-rays had energies of 30–50 keV, about the same energy as X-rays used today for medical diagnostics. Astronomical X-rays are much less energetic and more easily absorbed. Most X-rays from cosmic sources cannot penetrate even the thin outer layers of the Earth's atmosphere. It is thus impossible to observe X-rays from astronomical sources with ground-based instruments. Even from mountain tops, airplanes, and simple balloons, attempted observations are hopeless. Hence, observing from above the atmosphere is essential in this field. To see any X-rays at all, it is necessary to be above 99 per cent of the atmosphere, and to detect X-rays in the band where sources are most prominent, all but one millionth of the atmosphere must be below the instrument.

Cosmic X-ray sources are most clearly detected in the range of 0.5–5 keV in photon energy (or wavelength of 25–2.5 Å). By earthly standards, these X-rays are 'soft' and easily stopped by a small amount of material. For example, three sheets of paper or 10 cm of air at one atmosphere pressure will stop 90 per cent of 3 keV X-rays. The higher the energy, however, the more penetrating, or harder, the X-rays. A rocket is needed to observe 3 keV X-rays, which cannot be seen at altitudes below 80 km, whereas 30 keV photons will penetrate to 35 km altitude, which can be reached by the highest-flying balloons. The instrument should be above 200 km to observe X-rays with energies below 1 keV in a direction parallel to the Earth's surface, as would be desirable in a survey. A few cosmic sources emit hard X-rays and have been observed with balloons but almost all work is now done with satellite-borne instruments.

It was not a trivial matter to build the first instruments that were large enough to be sensitive yet small enough to fit within a rocket or balloon payload. The instruments not only had to withstand the rigours of launch but also had to operate in a vacuum or near vacuum. Time and trial and error were needed to develop the first survey instruments. To detect, for the first time, a phenomenon that many people believed impossible, took confidence that the instruments were operating properly. Much of the early work was done by nuclear physicists, who were familiar with the type of detectors used to register the X-rays.

Because X-rays are a form of electromagnetic radiation like visible light, they can be produced by the same processes. Because the photon energies are 1000 times greater than that of optical photons, the process must be correspondingly more energetic to produce X-rays. So, if X-rays are generated in a thermal process, the temperature must be of the order of 1000 times greater than that in places where light is produced. Thus, a search for cosmic X-ray sources is a search for material at temperatures of millions of degrees, in contrast to the familiar stars with surface temperatures of thousands of degrees. Until 1962, very few astronomers believed that the Universe contained objects capable of generating detectable amounts of high energy radiation and little was expected from the first observations.

These ideas changed dramatically in the early 1960s with the discovery that there were indeed many discrete, powerful sources of astronomical X-rays. Some produce X-rays by processes unimagined until the observations forced people to consider new kinds of cosmic objects and new methods of energy production.

1.4 Electromagnetic radiation and the atmosphere

It is not an accident that our eyes operate in the narrow waveband 4000–8000 Å. Not only is a large fraction of the energy of the Sun radiated in this band but the Earth's atmosphere is almost transparent throughout this 4000 Å-wide waveband. Figure 1.1 shows the electromagnetic spectrum from radio waves to gamma-rays and depicts the depth to which each frequency can penetrate the atmosphere. Over twelve decades of the spectrum, from gamma-rays to the far infrared (FIR), there is only a very narrow band of radiation that reaches the Earth's surface essentially unscathed. The 'opacity' (potential to absorb) of the atmosphere is the principal difficulty facing astronomers wishing to study radiation from the stars at wavelengths outside the visible band. Until this century, the visible part of the spectrum was all that was available for study of the heavens. Only radio astronomy was able to develop at all using ground-based instrumentation, although it is now possible to undertake infrared observations from high altitude observatories through some windows less affected by water vapor.

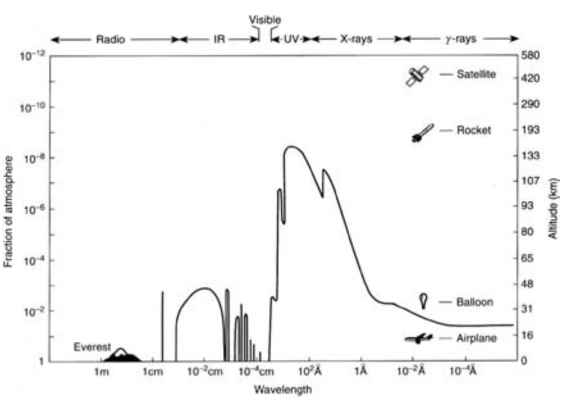

Fig 1.1 Transmission of electromagnetic radiation by the atmosphere. The solid line shows the altitude by which half the radiation from space has been attenuated. Just below this line virtually all the radiation is absorbed. Only radio, optical, and some narrow bands of infrared radiation can reach the Earth's surface. High energy γ-rays can be observed using balloons, but rockets or satellites are necessary for X-ray or UV detection.

Table 1.1 Atmospheric transmission of X-rays.

altitude (km)	energy (keV)	transmission, source overhead	transmission, source 90° from vertical
40	20	0.15	0.00
40	30	0.64	0.00
150	1	0.98	0.64
200	0.2	0.99	0.82

Figure 1.1 shows the height above sea level to which radiation of each wavelength can penetrate. All radiation from the extreme ultraviolet (UV) (at 1000 Å) to X-rays to high-energy γ-rays (at 10^{-4} Å) fails to penetrate below an altitude of $\sim$30 km. It is the requirement of observing above the atmosphere that makes the study of the X-ray Universe a modern one. At 40 km altitude, typical for balloon flights, the atmospheric transmission of 30 keV X-rays from a source directly overhead will be $\approx$60 per cent. If the source is 60° from the vertical, transmission is $\approx$36 per cent. A source 90° from the vertical cannot be detected. (This direction is the 'horizon' on Earth's surface but, at high altitude, the actual horizon can be well below this direction.) Table 1.1 gives transmissions for other altitudes and energies. It shows that 20 keV is about the low energy limit of balloon-borne detectors and that a rocket has to be above $\sim$150 km to perform a useful scan. At 200 km, the transmission of even the softest X-rays is high. Because

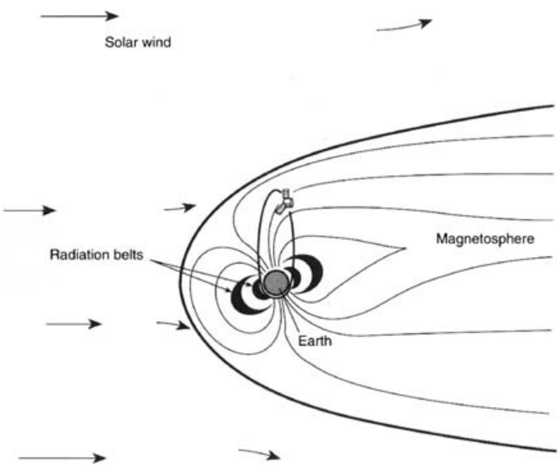

Fig 1.2 Earth and its magnetosphere. Magnetic field lines are connected to the Earth's poles and confined inside the bow shock, which is usually ~12 Earth radii distant in the solar direction. The inner and outer radiation belts are shaded. A spacecraft in the eccentric orbit shown spends most of its time above the intense zones of trapped particles but is always within the magnetosphere.

satellites operate at higher altitudes to avoid atmospheric drag, atmospheric attenuation does not limit satellite X-ray surveys.

1.5 The environment in space

Two restrictions govern orbits selected for X-ray observatories: (i) although soft cosmic X-rays can be detected at altitudes above 150 km (reached easily by rocket), a satellite in a circular orbit must have an altitude greater than 400 km or the drag of the tenuous upper atmosphere will soon lead to a fiery re-entry and (ii) because X-ray detectors are sensitive to energetic charged particles, observations are best done where particle fluxes (and detector backgrounds) are at a minimum.

Figure 1.2 shows (not to scale) the space environment in the vicinity of Earth. Inside the parabolic magnetopause, space is dominated by Earth's magnetic field. Outside, energy from the Sun, in the form of solar wind, magnetic field, and energetic particles, governs conditions. A bow shock forms just outside the magnetopause. The solar side of the magnetosphere boundary is normally 10–12 $R_{\oplus}$ (Earth radii) distant but can be pushed closer by solar activity. At a lower altitude, Earth is girdled by the pitted-olive shaped Van Allen radiation belts. Here, protons and electrons trapped in the Earth's magnetic field have both high energy and long lifetimes. The best orbits for observation minimise time spent in these zones, which extend from ~0.2–5 $R_{\oplus}$. Indeed, detectors must be powered off so as to prevent damage when in the heart of the belts.

A near-Earth equatorial orbit with altitude ≈500 km is below the belts except for a region over the South Atlantic Ocean where Earth's field is weak and trapped particles dip to lower altitudes. Earth's field keeps solar particles from this equatorial region and reduces the flux of cosmic rays. In addition, the solid Earth stops half the high-energy cosmic rays that penetrate the magnetic field. The consequent low background is an advantage, but in a near-Earth orbit, only half the sky is visible at any one time. Except for targets near the poles of the orbit, this means that the observations will be repeatedly interrupted for a large part of every ≈100-min orbital period. (This is exactly what happens with the Hubble Space Telescope.) Also, all detectors have to be turned off when passing through the South Atlantic Anomaly where charged particle flux is high. This causes another interruption on many orbits. Near-Earth polar orbits have also been used, usually because of launch site or data-receiving station locations. In these orbits, particle-induced backgrounds are low at low latitudes but high in polar regions due to precipitating solar and auroral particles.

A highly eccentric elliptical orbit will allow the spacecraft to spend almost all of the time well above the Van Allen zones. If beyond the magnetosphere, however, there is no protection from solar particles of all energies and background rates can be high after solar flares. Indeed, exceptionally large flares on the Sun can inject a huge number of energetic particles out into the Solar System. These affect the Earth by causing telecommunication problems and also spectacular auroral displays at high latitudes. Such a large flare can sometimes result in the need to turn spacecraft instruments off for several days, whereas within the magnetosphere, some shielding is provided from solar particle events. No orbit is free from transient solar particle fluxes and spacecraft operators must be vigilant to avoid damage to the sensitive detectors.

1.6 The early years (1946–1962)

The first technology useful for research above the atmosphere was that of the V2 rockets available after World War II. With these, the U.S. Naval Research Laboratory (NRL), under the direction of Herbert Friedman, was able to reveal the Sun as a powerful source of UV and X-radiation. Perversely, this discovery actually caused many scientists to lose interest in the search for other sources of X-rays, as they realised that the Sun appears as a bright source only because it is extremely close to us. A calculation of the intensity of radiation expected at the Earth from the nearest stars (assuming that they are comparable emitters of X-rays to the Sun) showed that the instrumentation available in 1960 would have had to be about a factor of 10^5 more sensitive to detect such objects. Worse still, if the stars were more distant, at a typical distance of 1 kiloparsec (kpc) or about 3000 light years, then a 1960 observation would only have been capable of discovering a process which was producing 10^{11} times the X-ray luminosity of our Sun.

Most of the rocket observations of the 1950s were devoted to more detailed studies of the Sun, although the NRL group did search (without success) for other cosmic sources. Even so, several groups kept working to develop more sensitive instruments. In the end, it was a group at American Science and Engineering (AS&E), led by Riccardo Giacconi, that was successful in the first detection of a powerful cosmic source of X-radiation.

1.7 Sco X-1

The official purpose of the AS&E experiment was to search for X-rays from the Moon, which were expected to be produced by the energetic solar wind particles striking the lunar surface, with perhaps some fluorescence from solar X-rays. A positive result would provide valuable information about the nature of the lunar surface; an area receiving much publicity and support at the time with America's commitment to a manned lunar landing within the decade. In addition, it was planned to scan a large region of sky in a search for non-solar sources of X-radiation. The first launch of this new instrument took place in October 1961. The rocket launch was perfect but the doors, designed to protect the X-ray detectors during launch and passage through the atmosphere, failed to open! In the early days, equipment was simple but often unreliable.

The second launch of the AS&E instrument, on a new Aerobee rocket, took place from White Sands, New Mexico, on 18 June 1962 and this time the doors functioned perfectly. Two of the three X-ray Geiger counters worked well and, although they failed to detect any X- rays from the Moon's surface, they made the first detection of a powerful cosmic X-ray source (Giacconi, Gursky & Paolini, 1962). This source subsequently became known as Sco X-1, the first-discovered source in the constellation Scorpius. As Richard Hirsch (1983, p. 46) comments in his history of X-ray astronomy, 'Observing Sco X-1 was the reward nature offered to scientists willing to gamble on a long shot'.

Interpretation of the data was not straightforward. With this detector, precipitating electrons could produce a signal similar to that of an X-ray source. By realising that the observed signal of 100 photons $cm^{-2}\ s^{-1}$ was indeed caused by an extrasolar X-ray source, Giacconi and colleagues captured the interest of the astronomical community and started an exploration that has uncovered some truly remarkable objects.

The unusual nature of Sco X-1 was clear as soon as it had been roughly located. Figures 1.3 and 1.4 contrast the X-ray and optical appearance of Sco X-1. The source dominates an early rocket X-ray survey. An optical picture, however, containing Sco X-1 shows nothing unusual whatsoever. Until an accurate location of the X-ray source was obtained (Gursky *et al.*, 1966), astronomers had not a clue as to the nature of this source. Sco X-1 is an object which stands out like a beacon to a small X-ray detector but is visually four hundred times fainter than the faintest star that can be seen with the naked eye. In every square degree of

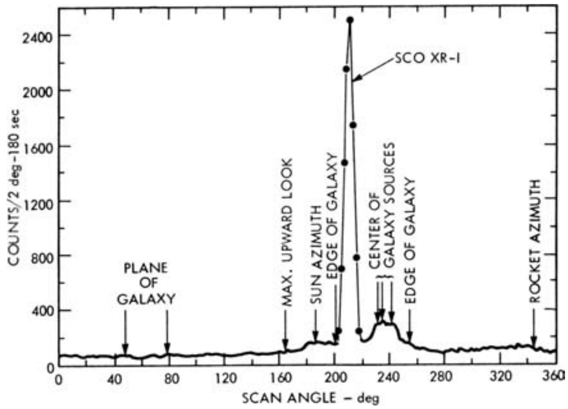

Fig 1.3 Three minutes of data from a rocket-borne X-ray detector flown in October 1967. This shows the counting rate of the detector as it scanned a great circle containing the source Sco X-1 and a cluster of sources in the direction of the galactic centre. The detector field of view was 5° by 30°. The Sun was below the horizon. The signal from Sco X-1 is very strong. (from Hill *et al.*, 1968).

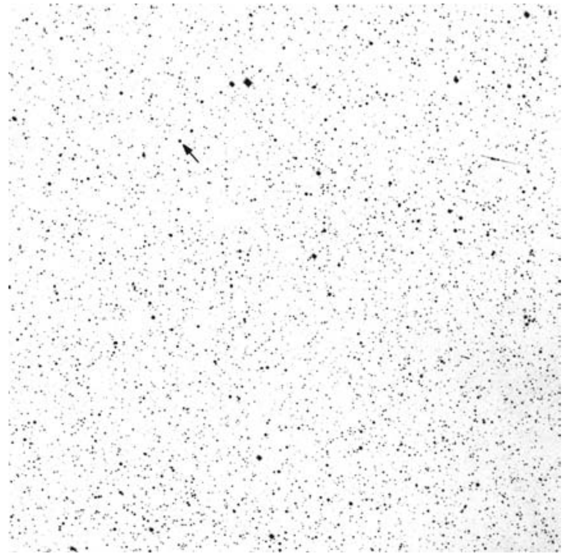

Fig 1.4 One square degree of the sky from the Palomar Sky Survey. The 13th magnitude star indicated with an arrow is the optical counterpart of Sco X-1.

the sky there are about one hundred stars visually brighter than Sco X-1.

1.8 An early history of the X-ray sky

After the discovery of Sco X-1, X-ray astronomy progressed rapidly. Evidence for two weaker sources was found on 12 October 1962 by the AS&E group (Gursky *et al.*, 1963). The NRL group confirmed and located one of these sources on 29 April 1963 using a rocket-borne detector (Bowyer *et al.*, 1964). It was identified right away as the Crab Nebula, a well-known young supernova remnant in our galaxy, and high energy X-rays from this source were detected on 21 July 1964 by George Clark (1965) of the Massachusetts Institute of Technology (MIT). (This was the first detection of high energy radiation from an extrasolar source with a balloon-borne detector.)

Astronomers were thus forced to recognise that there were many objects at stellar distances which were strong, unbelievably strong, sources of high energy photons. Small areas of the sky were then explored with great enthusiasm using rockets and balloons. The 'big picture' was not revealed until the first survey with the Uhuru satellite, launched on 12 December 1970.

The nature of the X-ray sources and the manner in which energy was generated was not obvious. It was first necessary to obtain precise locations of X-ray sources, leading to identification with optical or radio objects. The next steps were to measure the X-ray spectra and light curves to determine the emission mechanism.

Some of the brighter sources in our Galaxy radiate 10 000 times as much energy as does the Sun across all wavelengths. Almost all (99.9%) of this energy appears as X-rays. Sco X-1 is such a source. The optical counterpart is a 13th magnitude star, invisible to the naked eye and even to small telescopes. The only visual clues to its unusual nature are a blue-violet colour and an irregular variability marked by occasional rapid flickering. No optical surveys previous to the X-ray detection had indicated anything unusual. Even after the optical counterpart had been identified, the Sco X-1 system was not understood.

A convincing explanation of its nature was not found until 1971 when Uhuru discovered and measured the peculiar X-ray variation of another source that lies in the southern sky in the constellation Centaurus. This source, Cen X-3 (or 4U1118-60), is an X-ray-bright object at a declination of -60°. Although bright enough to be detected by a rocket-borne instrument, it was below the horizon for sounding rockets launched from the main U.S. facility at White Sands. It was clearly accessible, however, to those using launchers in Hawaii and Australia.

In 1967–1968, two groups surveyed the southern sky. A group from Lawrence Livermore Laboratory (LLL) detected Cen X-3 twice and derived a rough location (Chodil *et al.*, 1967). Figure 1.5 shows data from one of these flights. However, a group from Leicester observed twice and did not see it (Cooke & Pounds, 1971).

In the late 1960s it was no easy task to build detectors, calibrate them, ensure that they survived the quick but hazardous trip into space, and know where they were pointed. People took pride in their ability to distinguish real sources from the background and expected the source population to be more or less steady, like the stars. In the case of Cen X-3, both groups secretly suspected that the other had not interpreted the data properly. In truth, all these observations were carefully done and correctly interpreted. The source is highly variable. To a small detector, sometimes it appears above background and sometimes not. Furthermore, such variability is a common characteristic of most bright X-ray sources. It took a while for people to believe this.

The Uhuru observations of Cen X-3, made in 1971, were spectacular (Giacconi *et al.*, 1971; Schreier *et al.*, 1972). The X-ray observations alone determined the nature of the source.

The first surprise was the observation of a regular periodicity of 4.84 seconds in X-ray flux from Cen X-3. The modulation was high and the pulsations were easily seen during a single scan across the source. Only a rotating neutron star could produce such rapid pulsations. The period was measured accurately and it was soon discovered that the period varied slightly with time. After several days of data were collected, these variations were recognised as a Doppler shift. The neutron star was moving in a circular orbit with a period of only 2.09 days. As icing on the cake, the X-rays were observed to disappear completely for 11 hours at regular 2.09 day intervals. The source was in an eclipsing binary system.

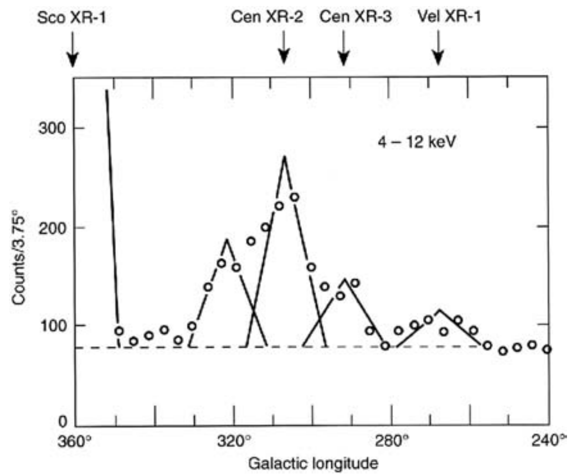

Fig 1.5 Counting rate from a rocket-borne proportional counter flown in May 1967. A slat collimator restricted the field of view to be 10° x 30°. The spinning payload caused the detector to scan a band of the sky repeatedly. By comparing the observed count rate with the expected triangular response to a point source, sources could be located. Sco X-1 was very bright and is off scale at 360°. The next strongest source at this time was Cen X-2, a transient. The source Cen X-3 was first seen in the data shown here. Note the difficulty of determining source positions in crowded regions (from Chodil *et al.*, 1967).

Here then was a rapidly spinning neutron star, probably emitting X-rays from the near-vicinity of one of its magnetic poles. It orbits a bright B0Ib star, Krzeminski's star (named after the person who identified the optical counterpart). Energy to power the X-ray source comes through accretion of material supplied by the supergiant companion. This matter is captured by the strong gravitational field of the neutron star. It acquires enough energy in the fall to the surface to both heat material to the high temperature required for X-ray emission and to supply the observed luminosity (see Chapter 11).

The other bright X-ray sources in the plane of our Galaxy were first detected in early rocket surveys (e.g. Figures 1.5 and 1.6). Most were found by groups at Lockheed (Fisher *et al.*, 1968), MIT (Bradt *et al.*, 1968) and NRL (Friedman *et al.*, 1967). The sources are mostly accretion-powered binaries, in which a normal star and a compact star are locked in a close orbit. Some, like Cen X-3,

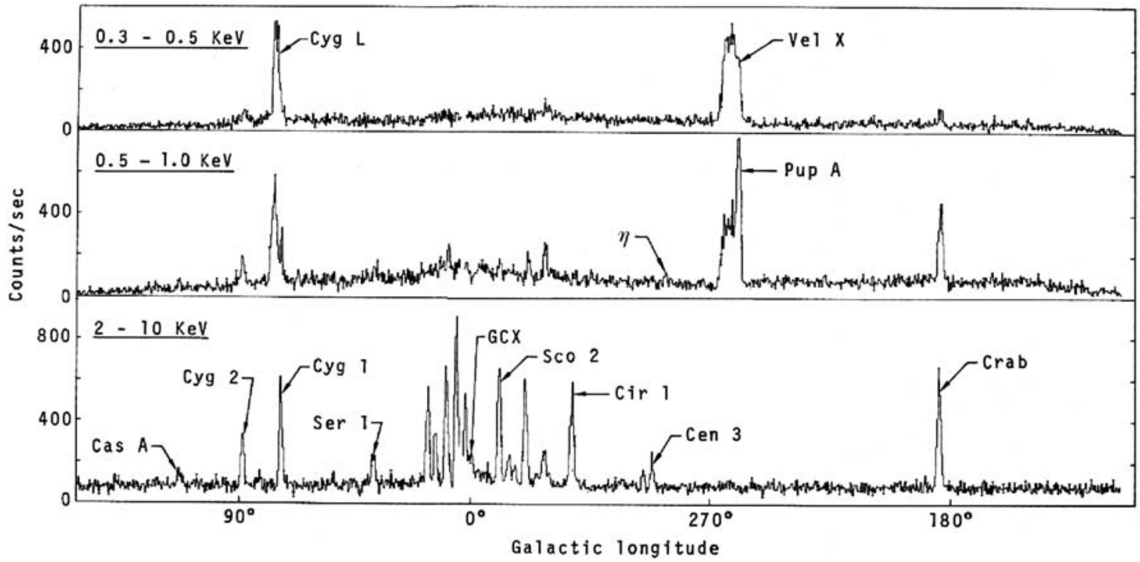

Fig 1.6 The entire Milky Way as surveyed with rocket-borne proportional counters in May 1970, May 1971, and October 1972 (Seward *et al.*, 1972). Collimation was 1.3° × 20°. Data from the three flights have been combined to show counting rate as a function of galactic longitude in three energy bands. There are no soft X-rays observed from the cluster of bright sources around the galactic centre. Intervening gas absorbs the soft X-rays. The nearby supernova remnant Vela XYZ is clearly soft and extended. These data were taken using the payload shown in Colour Plate 1, which was recovered and refurbished after each flight (figure available from FDS).

consist of a neutron star and a bright O star. The optical identifications of these were quickly made. Because the O stars are physically large, eclipses of the X-ray source associated with the orbiting neutron star are not unusual. Other sources consist of dim late-type stars orbiting close to a neutron star. These optical counterparts are faint and difficult to identify. The accretion-powered sources are the most luminous in our galaxy. Some have X-ray luminosities, $L_x \approx 10^{38}$ erg s^{-1}.

Some bright sources were found by Uhuru to be within globular clusters. Clark and colleagues (1975) found more with the third Small Astronomy Satellite (SAS 3) and pointed out that this was an unusual situation. The sources occur with much higher frequency than predicted by calculations based on the ratio of stars to X-ray sources in our galaxy (Clark *et al.*, 1975). The high stellar density in globular clusters is clearly favourable for the formation of these exotic binary systems (see Chapters 11 and 12).

In 1973, soft X-rays from SS Cygni were discovered by Rappaport *et al.* (1974). SS Cyg is a cataclysmic variable (CV) and is one of the brightest and nearest of this class. It has irregular outbursts during which the star brightens from its normal 12th to 8th magnitude. SS Cyg has been monitored by the American Association of Variable Star Observers (AAVSO) since 1896. It has an outburst about every 2 months and is called a *dwarf nova*. Many CVs are now known to be X-ray sources. They are accreting binary systems consisting of a low-mass normal star and a white dwarf (see Chapter 10).

Supernova remnants are bright X-ray sources, such as the first to be detected, the Crab Nebula. The X-ray luminosity of most remnants is 10–100 times less than that of the Crab Nebula and the spectrum is soft, so absorption in interstellar gas is more severe. Nevertheless, the closer remnants were easily detected and positively identified by their spatial extent (e.g. Cygnus Loop and Vela XYZ as seen in Figure 1.6) (Grader *et al.*, 1970) or by the spatial coincidence with a non-thermal radio source such as Cas A (Gorenstein *et al.*, 1970) (see Chapter 8).

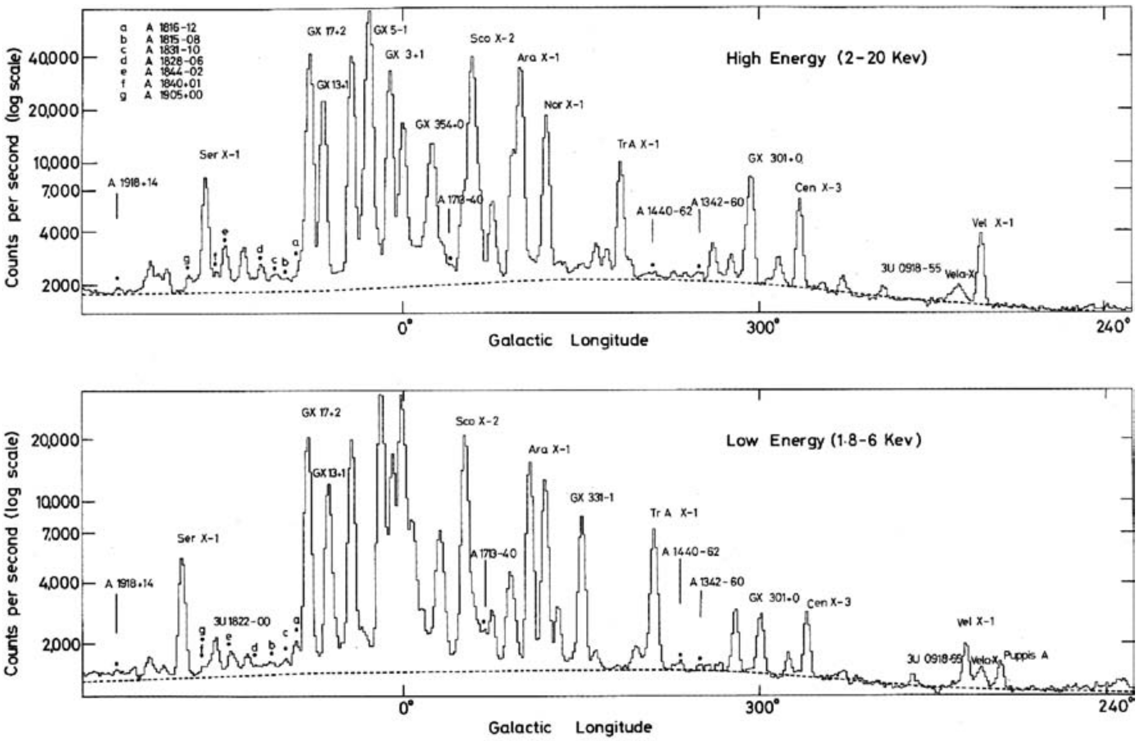

Fig 1.7 An Ariel 5 scan of the central half of the galactic plane. Two detectors scanned the sky, each with 0.7° x 10° field of view. The two collimators were inclined at different angles to aid in source location, so given sources do not appear at identical longitudes in this figure. Note the improvement in the ability to detect weak sources. (Courtesy of K. Pounds.)

Another class of sources are stars, binary perhaps, but without compact companions. The first indication of strong coronal emission from stars was obtained in April 1974 (Catura *et al.*, 1975). The X-ray luminosity was 10 000 times the X-ray luminosity of the Sun. The detection occurred by accident when the rocket-borne instruments were pointed at Capella to calibrate star sensors included in the payload for an accurate measure of pointing direction. Shortly afterwards, in October 1974, X-ray emission from a second star, the flare star YZ Canis Minoris, was observed with the ANS by Heise *et al.* (1975).

Because a bright star in an error box was a very tempting identification, false claims of X-ray detection of bright stars were not uncommon. In spite of this, it was soon evident that the coronal X-ray emission of many active stars was considerably more intense than that of our Sun (see Chapter 6).

As the sensitivity of observations increased, other sources were discovered that were not in our Galaxy. The first extragalactic source discovered was the active galaxy M87. The observation was made by Byram *et al.* (1966) with a rocket launched April 1965. In 1971, Uhuru added many quasars, active galaxies, and clusters of galaxies (Giacconi, 1974). Thus, the individual X-ray source populations were recognised as sources and identified.

Large fractions of the sky were surveyed by the first satellites devoted to X-ray astronomy. After Uhuru, SAS 3 and Ariel 5, a few hundred sources had been catalogued (e.g. Figure 1.7). The first satellite/observatory specifically designed for an all-sky survey was HEAO-1 in 1979, which used an array of large-area proportional counters. The result, shown in Colour Plate 2, was a catalogue with limiting sensitivity of 0.003 photons cm^{-2} s^{-1} containing 842 sources (Wood *et al.*, 1984). Ten years later, ROSAT mapped the sky for the first time using an imaging telescope and low-background detector. The threshold of this, the most sensitive X-ray all-sky survey to date, was 1.5×10^{-4} photons cm^{-2} s^{-1}, and the first version of the ROSAT catalogue contained more than 18 000 sources, both galactic and extragalactic (Voges *et al.*, 1999). Colour Plate 3 shows the ROSAT all-sky survey.

Flux and luminosity

Fluxes quoted are measured at the top of the Earth's atmosphere. To give an intuitive feeling for the X-ray brightness of a source, fluxes in this chapter have been quoted in units of photons cm^{-2} s^{-1}. The counting rate of an X-ray detector, $C = F_p \epsilon A$, where F_p is photon flux, ϵ is detector efficiency and A is detector area integrated over the energy range of the detector. Because detector efficiencies usually ranged from 0.1 to 1.0, and detector areas from 100 to 1000 cm^2, the counting rate of early X-ray detectors was ~100 times the photon flux quoted.

To be more precise, we should specify an energy flux (ergs cm^{-2} s^{-1}) and the exact energy range covered. The observed flux is a measure of the brightness of a source. The intrinsic luminosity, L, is related to the flux, F, through the square of the distance to the source, d. Thus, $L = 4\pi d^2 F$. As a matter of interest, in the range 0.2–10 keV, one of the most luminous X-ray sources known is the quasar PKS 2126-150, at a red shift of 3.27 and with $L_x = 5 \times 10^{47}$ erg s^{-1}. One of the least luminous extra-terrestrial X-ray sources detected is the Earth's Moon with $L_x = 7 \times 10^{11}$ erg s^{-1}, a range of physical processes that produce X-ray emission varying by 36 orders of magnitude.

In a more selective mode of operation, X-ray telescopes have accomplished deep surveys of small regions of the sky. The Einstein and ROSAT deep-survey detection thresholds were $\approx 3 \times 10^{-5}$ and $\approx 1 \times 10^{-5}$ photons cm^{-2} s^{-1}, respectively. The XMM and Chandra limits are 100 times fainter again or ≈ 3 photons m^{-2} hr^{-1}. This is 1 billion times fainter than Sco X-1, the brightest source in the sky. (Actually, at energies above ~1 keV, transient sources up to twice as bright as Sco X-1 have been observed. Below ~1 keV, as you know, the Sun is the brightest source in the sky.)

References

Observation

Bradt, H., S. Naranan, S. Rappaport & G. Spada (1968) Celestial positions of X-ray sources in Sagittarius, *ApJ* **152**, 1005.

Bowyer, S., *et al.* (1964) X-ray sources in the galaxy, *Nature* **201**, 1307.

Byram, E., T. Chubb & H. Friedman (1966) Cosmic X-ray sources, galactic & extragalactic, *Science* **153**, 1527.

Catura, R. C., L. W. Acton & H. M. Johnson (1975) X-ray emission from Capella, *ApJ* **196**, L47.

Chodil, G., *et al.* (1967) Spectral and location measurements of several cosmic X-ray sources including a variable source in Centaurus, *Phys. Rev. Letters* **19**, 681.

Clark, G. W. (1965) Balloon observation of the X-ray spectrum of the Crab Nebula above 15 keV, *Phys. Rev. Letters* **14**, 91.

Clark, G. W., T. H. Markert & F. K. Li (1975) Observation of variable sources in globular clusters, *ApJ* **199**, L93.

Cooke, B. A. & K. A. Pounds (1971) Further high sensitivity X-ray sky survey from the Southern Hemisphere, *Nature Phys. Sci.* **229**, 144.

Fisher P. C., *et al.* (1968) Observations of galactic X-ray sources, *ApJ* **151**, 1.

Friedman, H., E. T. Byram & T. A. Chubb (1967) Distribution and variability of cosmic X-ray sources, *Science* **156**, 374.

Giacconi, R., H. Gursky, F. Paolini & B. Rossi (1962) Evidence for X-rays from sources outside the Solar System, *Phys. Rev. Letters* **9**, 439.

Giacconi, R., *et al.* (1971) Discovery of periodic X-ray pulsations in Centaurus X-3, *ApJ* **167**, L67.

Giacconi, R., *et al.* (1974) The Third UHURU Catalog of X-Ray Sources, *ApJ Supp* **27** 37.

Gorenstein, P., E. Kellogg & H. Gursky (1970) X-ray characteristics of three supernova remnants, *ApJ* **160**, 199.

Grader, R. J., R. W. Hill & J. P. Stoering (1970) Soft X-rays from the Cygnus Loop, *ApJ* **161**, l45.

Gursky, H., R. Giacconi, F. Paolini & B. Rossi (1963) Further evidence for the existence of galactic X-rays, *Phys. Rev. Letters* **11**, 530.

Gursky, H., *et al.* (1966) A measurement of the location of the X-ray source Sco X-1, *ApJ* **146**, 310.

Heise, J., *et al.* (1975) Evidence for X-ray emission from flare stars observed by ANS, *ApJ* **202**, L73.

Hill, R. W., R. J. Grader & F. D. Seward (1968) The soft X-ray spectrum of Sco XR-1, *ApJ* **154**, 655.

Rappaport, S., *et al.* (1974) Possible detection of very soft X-rays from SS Cygni, *ApJ* **187**, L5.

Schreier, E., *et al.* (1972) Evidence for the binary nature of Centaurus X-3 from Uhuru X-ray observations, *ApJ* **172**, L79.

Seward, F. D., *et al.* (1972) Distances and absolute luminosities of galactic X-ray sources, *ApJ* **178**, 131.

Catalogues, reviews

Hirsch, R. F. (1983) *Glimpsing an Invisible Universe*, Cambridge: Cambridge University Press.

Tucker, W. H. & R. Giacconi (1985) *The X-ray Universe*, Cambridge, MA: Harvard University Press.

Voges, W., *et al.* (1999) The ROSAT all-sky survey bright source catalogue, *A&A* **349**, 389.

Wood, K. S., *et al.* (1984) The HEAO A-1 X-ray source catalog, *ApJ Supp* **56**, 507.

Chapter 2

X-ray emission and interaction with matter

2.1 Astrophysical mechanisms for generating X-rays

There are three radiation processes – thermal, synchrotron and blackbody – that are the dominant mechanisms for producing X-rays in an astronomical setting, and whenever high-energy electrons are present, we must add inverse Compton scattering of microwave background photons into the X-ray regime. The spectral signature of each process is unique and is therefore one of the first clues to the nature of an unknown X-ray source. If the spectrum can be measured with high resolution over a broad energy band, then usually both the emission process and the physical conditions within the source can be deduced.

2.1.1 Thermal emission from a hot gas

Consider a hot gas of low enough density that it can be described as thin and transparent to its own radiation. This is not difficult to achieve for X-rays. At temperatures above 10^5 K, atoms are ionised, and a gas consists of positive ions and negative electrons. Thermal energy is shared among these particles and is transferred rapidly from one particle to another through collisions. Indeed *thermal equilibrium* means that the average energy of all particles is the same and is determined only by the temperature. When an electron passes close to a positive ion, the strong electric force causes its trajectory to change. The acceleration of the electron in such a collision causes it to radiate electromagnetic energy, and this radiation is called *bremsstrahlung* (literally, 'braking radiation').

Electrons in thermal equilibrium have a well-determined distribution of velocities (called *Maxwellian* after the physicist James Clerk Maxwell), and the radiation from such electron-ion collisions is a continuum with a characteristic shape determined only by the temperature. This is *thermal bremsstrahlung*. The higher the temperature, the faster the motion of the electrons and hence the higher the energy of the photons in the bremsstrahlung radiation. For temperatures above 1 million degrees, these photons are predominantly X-rays.

The thermal bremsstrahlung spectrum falls off exponentially at high energies and is characterised by the temperature T. The intensity, I, of the radiation at energy E is given by

$$I(E, T) = AG(E, T)Z^2 n_e n_i (kT)^{1/2} e^{-E/kT},$$

where k is Boltzmann's constant and G is the *Gaunt factor*, a slowly varying function with value increasing as E decreases. The form of this spectrum can be seen in Fig. 2.1. Note that the intensity is proportional to the square of the charge of the positive ions, Z, and the product of the electron density, n_e, and the positive ion density, n_i. A is a constant.

In a hot gas, X-ray line emission is also an important source of radiation. The elements heavier than hydrogen are not completely ionised, except at very high temperatures ($\geq 5 \times 10^7$ K). When a fast electron strikes an ion with bound electrons, it often transfers energy to that ion, causing a transition to a higher energy level. The

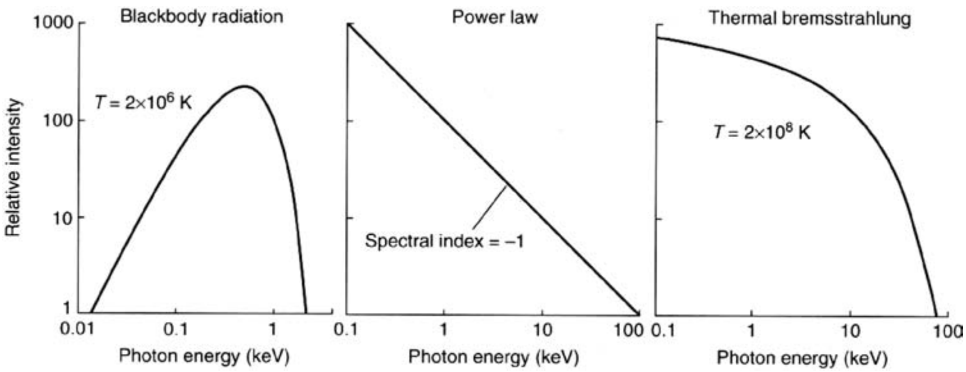

Fig 2.1 Spectral forms expected from different astrophysical processes.

ion is left in an excited state which lasts only briefly. The ion decays to its ground state by radiating photons of energy characteristic of the spacing of energy levels through which the excited electron passes. This radiation appears as spectral lines with energies determined by the radiating ion species.

Radiation from a thermal gas is thus a blend of thermal bremsstrahlung and line radiation (other processes also make small contributions, but X-ray diagnostics usually rely on these two). For a gas of 'cosmic' composition (which, for every 10 000 atoms of hydrogen, contains 850 atoms of helium and 16 atoms of carbon, oxygen and heavier elements), at temperatures below 10^6 K, most of the energy is radiated as UV lines. At 2×10^6 K, half the energy is radiated as soft X-rays; at 10^7 K, all the energy is radiated as X-rays, half in lines and half as thermal bremsstrahlung. At 5×10^7 K, almost all the ions have been stripped of their bound electrons, and almost all the energy is radiated in the X-ray continuum. Figure 2.2 shows how ion state depends on temperature.

Thus, by measuring X-ray spectra, the shape of the continuum and/or the presence of lines can identify the origin as a hot gas. The temperature of the gas can be calculated from the particular lines present and from the shape of the high-energy end of the bremsstrahlung continuum. The strength and energies of the lines reveal the elemental composition of the gas.

The power, P, radiated by 1 cm^3 of cosmic-composition gas at uniform temperature is given by the cooling curve shown in Figs. 2.3 and 2.4. The luminosity of a volume, V, of this gas is $L = P(T)n_e n_i V$. If the distance of a diffuse X-ray source is known, the volume of X-ray-emitting gas can usually be estimated and the gas density derived from this expression.

The quantity $n_e n_i V$ is called the *emission measure*. Astrophysical sources, such as stellar coronae, are seldom isothermal, and a source with volumes of gas at different temperatures is described by a *differential emission measure* (DEM). One definition is $\mathrm{DEM}(T) = n_e n_i \Delta V / \Delta T$. Although the definition varies a bit from paper to paper, the DEM is always used to give the temperature distribution of the emitting plasma. An example is shown in Chapter 6.

2.1.2 Synchrotron radiation from relativistic electrons

A fast electron traversing a region containing a magnetic field will change direction because the field exerts a force perpendicular to the direction of motion. Because the velocity vector changes, the electron is accelerated and consequently emits electromagnetic energy.

This is called *magnetic bremsstrahlung* or *synchrotron radiation* (after radiation observed from particle accelerators by that name). The frequency of the radiation depends on the electron energy, the magnetic field strength B and the direction of motion relative to the field.

In an astrophysical setting, the magnetic field can be somewhat aligned, but particle velocities are expected to be isotropic, so the observed

Fig 2.2 Ionic equilibrium of hydrogen, oxygen and iron in a thin gas as a function of temperature. At a temperature of 3000 K, all H atoms have a bound electron, whereas by 16 000 K, half the atoms are ionised. Above 30 000 K, no electrons are bound to H nuclei. As temperature rises, more and more electrons are stripped from the heavier atoms. These curves are recalculated whenever new atomic physics data are available, and recent calculations predict slightly different temperature dependences for Fe than shown here (taken from calculations of D. Cox and C. Jordan; see Jordan, 1969).

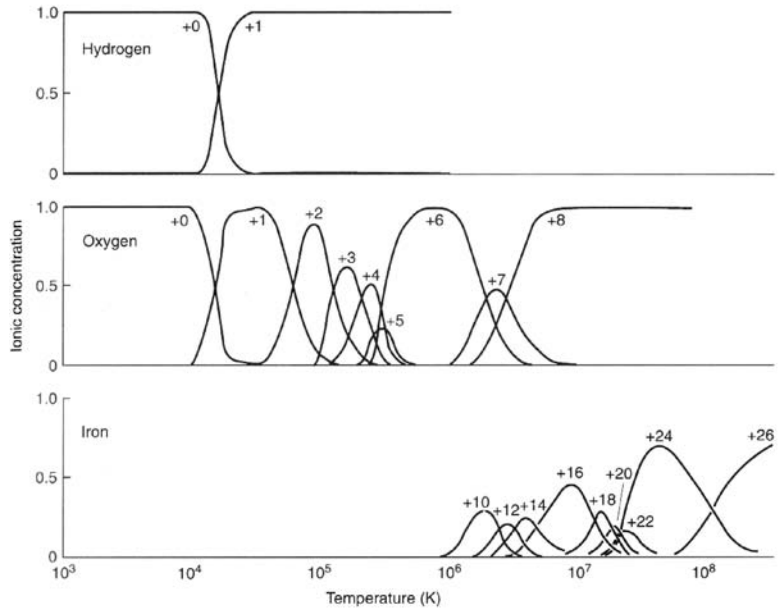

spectrum depends only on B and the energy spectrum of the electrons. The usual spectral form assumed for the electrons is a power law, and if this is so, then the spectrum of the resulting synchrotron radiation is a power law also. Indeed, when an observed spectrum is a power law over a reasonably large energy range, it is usually taken as a strong indication that the source is emitting synchrotron radiation. If the magnetic field is aligned, the radiation will be polarised, and observed polarisation is usually proof of synchrotron emission.

The form of the power-law spectrum is simply $I(E) = AE^{\gamma}$, where A is a constant and γ is the spectral index. The more negative the value of γ, the softer is the spectrum. The spectrum shown in Fig. 2.1 has $\gamma = -1$.

The power radiated as synchrotron radiation is proportional to B^2E^2 and the average photon energy to BE^2. In an astronomical setting, synchrotron X-rays indicate the existence of very energetic electrons. Two examples of such synchrotron radiation are (1) radio emission from shell-like supernova remnants where the magnetic field strength is $\approx 7 \times 10^{-5}$ Gauss and the electrons which radiate radio waves have energies of about 1 GeV; (2) the central region of the Crab Nebula where the magnetic field is $\approx$10 times stronger than this. Radiation is emitted over most of the electromagnetic spectrum, and the electrons which produce synchrotron X-rays here have energies of about 10^4 GeV, a few ergs each! Furthermore, because these electrons lose energy rapidly, there must be a continuous injection of fresh electrons, which is achieved by their being accelerated in the rapidly spinning pulsar magnetosphere (see Chapter 9).

The derivation of synchrotron emission assumes that electrons travel in a uniform magnetic field and at an angle to the field lines. There is no radiation when particles move parallel to the field lines. The field lines around a neutron star, for example, however, are not straight, and an electron moving along one of these lines will be accelerated and will radiate. This special case of synchrotron radiation is called *curvature radiation*.

2.1.3 Inverse Compton X-rays from relativistic electrons

An ultra-relativistic electron can collide with photons and produce X-rays. In the rest frame of the electron, there is Compton scattering, and the photon transfers energy to the electron. In the laboratory frame, the scattered photons are Doppler shifted to high energies, and the process is called *inverse Compton scattering*.

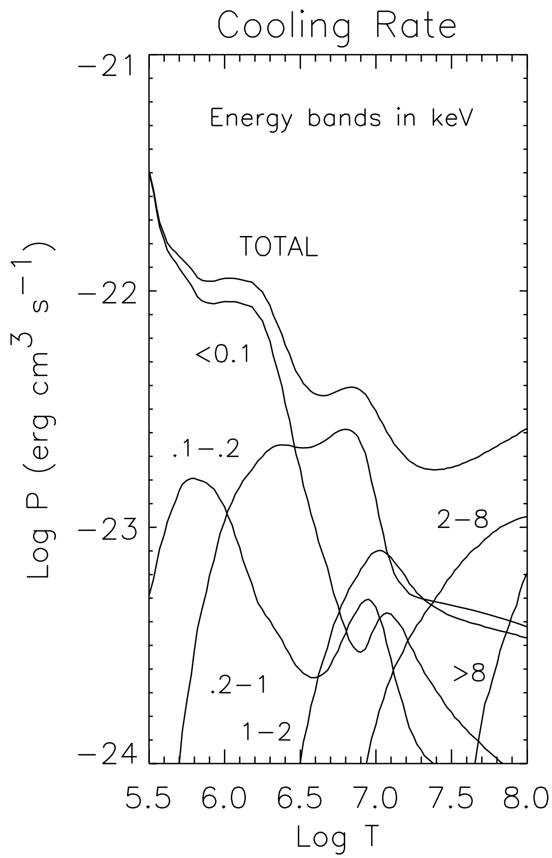

Fig 2.3 Power radiated from a low-density plasma as a function of temperature in several X-ray wavebands. Each curve is labelled with the energy range in keV. The material is in thermal equilibrium, and abundances are cosmic. The counter-intuitive result that the emission is stronger at *lower* temperatures is because of the contribution of emission lines, which disappear at higher temperatures as the atoms become completely ionised (figure from John Raymond; update of Raymond *et al.*, 1976).

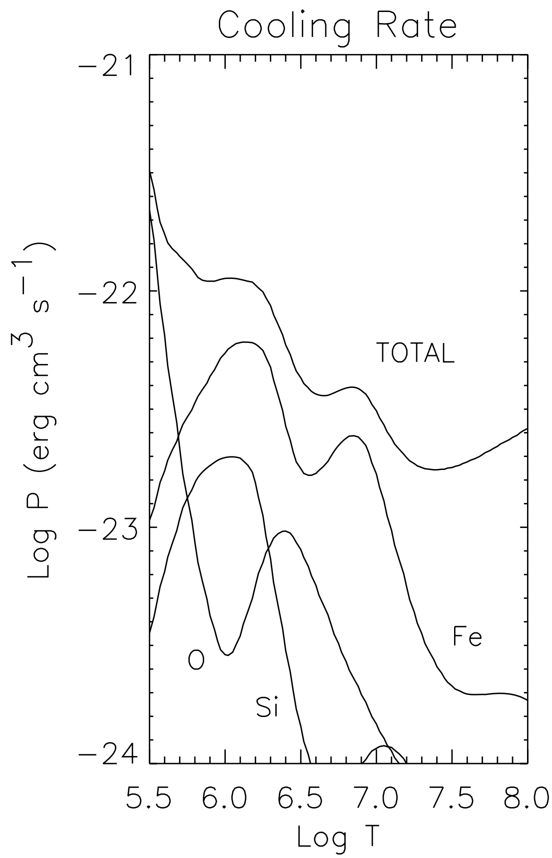

Fig 2.4 Power radiated from a low-density plasma as a function of temperature showing contributions because of collisional excitation from three elements (figure from John Raymond; update of Raymond *et al.*, 1976).

The total energy of a relativistic particle is γmc^2, where γ is the Lorentz factor, $[1 - (v/c)^2]^{-1/2}$. If the photon environment has energy density $u_{\rm rad}$ and photon energy is $h\nu$, the inverse Compton power radiated is proportional to $\gamma^2 u_{\rm rad}$ and the scattered photon has energy $\gamma^2 h\nu$. Thus cosmic-ray electrons with $\gamma = 1000$ will make keV X-rays when colliding with 10^{-3} eV cosmic microwave background (CMB) photons and MeV γ rays colliding with starlight. Because the CMB pervades all space, inverse Compton scattering is a serious energy loss for any ultra-relativistic particles traveling intergalactic distances. The process is also important in quasar jets where $u_{\rm rad}$ is high and high-energy particles are abundant.

2.1.4 Blackbody radiation from starlike objects

A 'black' surface completely absorbs any radiation incident upon it. Reflectivity is zero. It is furthermore a law of nature that the surface must not only absorb but also emit radiation. The spectrum radiated is a well-defined continuum with peak emission at an energy dependent only on the temperature, T. The higher the temperature, the more energetic the photons. A familiar example is the electric heating element on a stove or hot plate. As it is heated it first glows a deep red and then, as the temperature increases, becomes orange and almost yellow.

The form of the spectrum is given by

$$I(E,T) = 2E^3[h^2c^2(e^{E/kT} - 1)]^{-1},$$

where h is Planck's constant and c is the speed of light.

The stars radiate as blackbodies with temperatures from 2500 K (red dwarf) to 40 000 K (O star). Although strongly modified by the stellar atmospheres the spectra retain the overall gross shape imposed by the blackbody emission process. A newly formed neutron star is expected to have a very hot surface. If the surface temperature is 10^6 K or higher, it will emit blackbody radiation with photons in the X-ray range. The spectra of isolated neutron stars do have this form, but usually, strong magnetic fields at the surface cause complications.

2.1.5 Bombardment

This last process applies to much of Chapter 4. In the laboratory, X-rays are produced by bombarding a target with a beam of electrons. In the solar system, planets, moons and comets are bombarded with particles from the Sun and from planetary magnetospheres. The target emits bremsstrahlung X-rays and fluorescent X-rays with energies characteristic of the target and of any bombarding ions. Solar X-rays also bombard cold objects which emit scattered and fluorescent X-rays.

2.2 Interaction of X-rays with matter

When a beam of X-rays passes through a slab of material, some photons disappear from the beam. There is no gradual loss of energy, as for a beam of charged particles. X-rays collide with individual atoms, and the photon energy is deposited in surrounding material. The transmitted beam has fewer photons, but the energy of each transmitted photon has not changed. For a slab of thickness x, the intensity of the transmitted beam is reduced by a factor $e^{-\mu x}$, and μ is called the *absorption coefficient*. Working with solid materials on Earth, it is customary to use the density ρ to define a mass-absorption coefficient μ/ρ and to measure thickness in grams per centimeter squared. In astronomy, thickness is measured as the number of atoms N_H in a 1-cm^2 column between the observer and source, and the absorption coefficient becomes a cross section, usually written as σ. Hence the absorbing factor is usually written as $e^{-\sigma N_H}$.

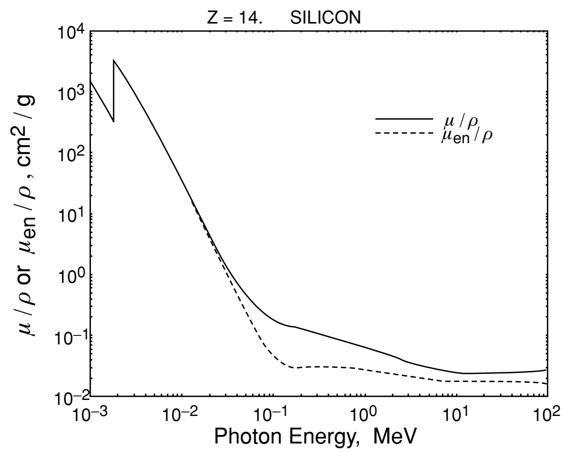

Fig 2.5 X-ray attenuation coefficient for Si as a function of energy from 1 keV to 100 MeV. The solid curve shows probability of X-ray interaction. The dashed line shows the fraction of the photon energy that is transferred to the kinetic energy of charged particles. Photoelectric absorption dominates at low energies and decreases rapidly as energy increases. At 1.839 keV, ejection of a K-shell electron is possible. At ≈30 keV, Compton scattering becomes important. Above ≈20 MeV, pair production is important (from Hubbell & Seltzer, 1996).

X-rays interact with matter in several ways. In the energy range 0.1–10 keV, the main interaction is the photoelectric effect. An atom absorbs the photon and ejects an electron with energy equal to that of the photon minus the binding energy of the electron, i.e. $E_{\mathrm{el}} = E_{\mathrm{ph}} - E_b$. The photoelectric cross section varies with energy as $\sim Z^3E^{-3}$, so absorption is greatest at low energies and in high-Z materials. For a given material, as photon energy increases, μ decreases, but when the energy becomes high enough to free one of the more tightly bound electrons, there is an abrupt increase in μ. Figure 2.5 shows the absorption coefficient energy dependence of one element (arbitrarily chosen to be Si). In the energy range 0.1–10 keV, X-ray interstellar absorption curves show 'edges' corresponding to the binding energies of electrons in the K and L shells of light elements. Figures 5.1 and 5.2 show these expected effects in the ISM.

X-ray photons also scatter from individual electrons within the atom. This process is called *Compton scattering* and is not important at low energies. In this process, the energy of the incident X-ray is shared between the scattered photon and the electron. The electron energy depends on the scattering angle and is maximum when the photon is scattered back in the incident direction. The maximum energy transferred to the electron is appreciable at high energies and very small at low energies. A 100-keV X-ray can transfer up to 28 per cent of its energy to a Compton electron. A 10-keV photon can transfer up to 4 per cent, and a 1-keV X-ray can transfer up to only 0.4 per cent (4 eV). (A third process becomes possible above 1.02 MeV. Here all the photon energy can go into production of an electron-positron pair. This is important for γ-ray detection but far above the energies considered in this book.)

So X-ray detectors in the range 0.1–10 keV respond to energy deposited by photoelectrons in the active volume of the instrument. At higher energies Compton electrons can also play a role. The next chapter concerns details of such detectors. X-rays also scatter from atoms as a whole with no energy loss. This occurs in diffraction gratings where the wave nature of X-rays is utilised for high-resolution energy measurements and at low incidence angles when X-rays are scattered from smooth surfaces, as in X-ray telescope mirrors, as discussed in the next chapter.

References

Hubbell, J. H. & S. M. Seltzer (1996) NIST tables of X-ray mass attenuation coefficients and mass energy-absorption coefficients, http://physics.nist.gov/PhysRefData/XrayMassCoef/ElemTab/z14.html.

Jordan, C. (1969) The ionization equilibrium of elements between carbon and nickel, *MNRAS* **142**, 501.

Raymond, J. C., D. P. Cox & B. W. Smith (1976) Radiative cooling of a low-density plasma, *ApJ* **204**, 290.

Chapter 3

Tools and techniques

3.1 X-ray detectors

The first instruments used for X-ray astronomy were developed originally for the detection of charged particles and γ rays emitted by radioactive material. These detectors respond to energy deposited by photoelectrons and, for higher energies, Compton electrons (discussed in Chapter 2). A fast electron creates a track of ionised material in the active volume of the detector. The detector collects either this charge or light from recombination of the ions. Electronic circuits then amplify this signal and record the time and amplitude of the event.

3.1.1 The proportional counter

The proportional counter is not only an efficient X-ray detector but also measures the energy of every photon detected. It was the workhorse of early cosmic X-ray observations and is still being used in modern instruments. However, the modifications necessary to adapt the simple laboratory counter to an X-ray detector capable of operating in the harsh environment of space were challenging.

The detector must have a large area to collect photons from weak cosmic sources and obviously a window thin enough to transmit X-rays. Yet the window has to be strong enough to keep the gas inside the detector from leaking into the near-vacuum of space and well supported to withstand the force of the gas pressure inside the detector. Many an early observation was lost by the failure of detector windows during rocket ascent out of the atmosphere and upon first exposure to space. A typical rocket-borne proportion counter, such as that shown in Fig. 3.1, had a window of 0.1 mm Be or of even thinner plastic, such as Formvar, and an area of 100–300 cm^2. The detectors were filled with a noble gas-methane mixture (A, Ne and Xe were used) at slightly more than 1 atmosphere pressure.

When an X-ray photon enters the detector through the thin window, it is absorbed by atoms of gas contained inside the counter. The resultant photoelectrons produce short tracks of ions and electrons inside the gas. These electrons are attracted towards and drift to the vicinity of the central wire or anode (maintained at about +2000 volts), where they cause further ionisations by colliding with other atoms. An avalanche of

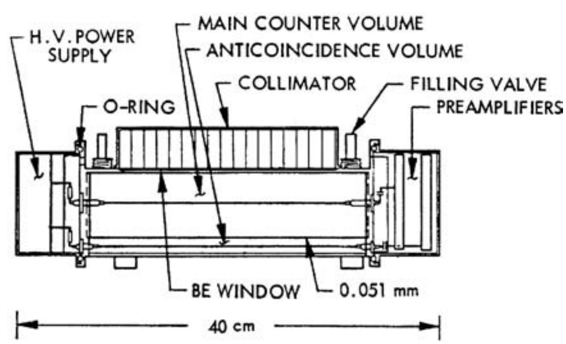

Fig 3.1 A proportional counter used in early sounding rocket observations. A slat collimator restricts the field of view, and the central volume is surrounded on three sides (one shown here) by guard counters to reject events caused by cosmic rays (from Chodil *et al.*, 1967).

Box 3.1 | Rejection of charged-particle events

Above the atmosphere a detector is bathed in a flux of charged particles: high-energy cosmic rays and sometimes trapped or precipitating particles. These produce background events in the detector which can overwhelm the weak signals from astronomical sources unless precautions are taken.

An X-ray photon can only enter the detecting volume by passing through the collimator and the thin entrance window. Cosmic rays, however, can pass completely through the walls of an X-ray detector and even through the spacecraft carrying it! In doing so, they deposit a line of charge through the counter gas which is then detected in the same way as that produced by real X-rays. A second detector, called a *guard counter*, is usually placed close to the X-ray detector. Most cosmic rays traversing the X-ray detector will also pass through the guard counter. Any event detected simultaneously in both volumes can be discarded by on-board electronic logic. The guard counter is said to be in *anti-coincidence* with the main X-ray counter or is being used as a *veto* system. Guard counters can be built into the same chamber as the X-ray detector so that they use the same gas supply. Sometimes several guard counters surround the X-ray detector on all sides.

An X-ray photoelectron makes a track $\sim$1 mm in length in the detector gas. This produces a short ($\leq$10 ns) rise-time pulse at the anode. A cosmic ray produces a much longer trail (several centimeters), and the charge therefore arrives at the anode spread over a much longer period of time ($>$100 ns). These times can be measured electronically for every event, and only short-rise-time X-ray events are admitted by the electronics. This technique for charged-particle event rejection is called *pulse rise-time discrimination*. The height (or amplitude) of the pulse can also be used as a discriminant to reject charged particles as they usually deposit considerably more energy in the detector than do X-rays.

Thus more than 90 per cent of cosmic-ray-induced events can be rejected. There are also low energy protons and electrons moving in the Earth's magnetic field that can penetrate the window and deposit a few keV in the detector. Magnets built into the collimator can sweep these into the collimator sides and prevent them from entering the window.

The flux of particles in the radiation belts surrounding the Earth is high, and astronomical detectors risk being severely damaged or destroyed if they are activated within that region. The resultant high count rates swamp the high voltage anodes, causing serious breakdown problems. Even near-Earth orbits can pass through a region known as the *South Atlantic Anomaly*, in which the charged particle flux is high enough to damage detectors. Precautions must be taken to operate a proportional counter on a satellite. Even rocket observations made at lower altitude can be troubled by precipitating electrons.

electrons occurs close to the anode, and the net result is a burst of electrons that are collected on the central wire. The avalanche amplifies the original signal (the number of electron-ion pairs created by the photoelectron) in a linear way. Events from the detector output, sorted by size, form a *pulse-height spectrum* which is clearly related to the energy of the incident X-rays (through the photoelectrons). Events from UV photons are discriminated against by rejecting all pulses below a certain threshold.

In a Geiger counter (as used in the original AS&E experiment) the voltage is higher, and the avalanche becomes a discharge which gives no more information than the fact that the event occurred. However, in the proportional counter the central wire is maintained at a slightly lower voltage so that the number of electrons collected by the anode is proportional to the energy of the incident X-ray photon.

3.1.1.1 Imaging proportional counters

Several techniques can be used to record the position of an event within a proportional counter. If the anode is a single wire, but made of resistive material, the position of the event along the length of the wire can be determined by the relative size of the pulse measured at the two ends of

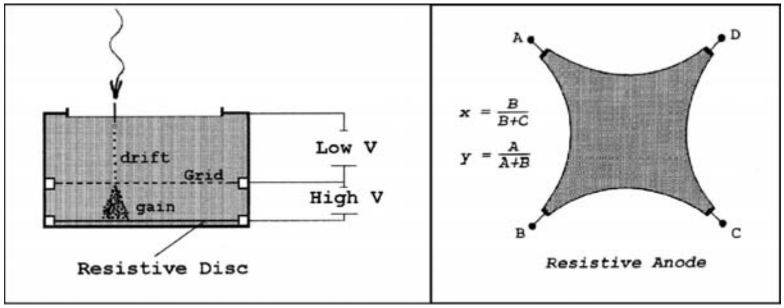

Fig 3.2 (left) A diagram of the position-sensitive proportional counter used on EXOSAT. The avalanche occurs close to the cathode so the charge is confined to a particular spot on the plate. (right) Signals from the corners of the plate are combined to measure the location of the event.

the wire. When used at the focus of a telescope, the counter becomes two-dimensional. Positive ions from the localised avalanche travel to the cathode and deposit their charge in a limited area close to where the avalanche occurred.

By making the cathode a resistive plate (as illustrated in Fig. 3.2) and measuring the size of the pulse at the four corners, the location of the deposited charge can be determined. This system was used in one of the EXOSAT detectors. Another technique used in the Einstein imaging proportional counter (IPC) was a cathode made of crossed resistive wire grids.

3.1.2 Gas-scintillation proportional counter

The gas scintillation proportional counter (GSPC), used on several missions, is similar in operation to a conventional proportional counter. Instead of detecting the electron cloud produced when the X-ray photon enters the counter, the GSPC detects the optical flash or scintillation that occurs when the ionised atoms in the gas recombine (i.e. rejoin with an electron). This process is analogous to that of the crystal-based scintillation counter used for detecting energetic X-rays. The avalanche is dispensed with and the intrinsic energy resolution is better than a standard proportional counter; it is close to that of a solid-state detector but without the need for cooling to very low temperatures.

3.1.3 The scintillation counter

Proportional counters do not detect photons with energies above 20 keV efficiently. This is because the detecting volume is a gas and, at high energies, the gas becomes transparent. A thicker (i.e. more absorbing) detecting medium is needed, and high-Z material is an advantage.

The scintillation counter uses crystals of sodium iodide or caesium iodide, which can efficiently stop photons with energies up to several MeV. The photon energy is absorbed by an atom within the crystal, and some of this energy immediately reappears as a pulse of light or *scintillation*. A photomultiplier tube then detects the scintillation, thus registering the time of the event. The amount of light in the scintillation is proportional to the incident X-ray photon energy.

For rejection of events caused by cosmic rays passing through the detector, the principal crystal was often surrounded by a second scintillating material. This could be in a separate light-tight assembly with its own photomultiplier. Because it is easily machinable, plastic scintillator was often used for the cup-shaped guard detector. However, the light pulses from plastic scintillator have faster risetimes than those from NaI or CsI. The NaI X-ray detector can be surrounded with plastic scintillator and all viewed by a single photomultiplier. The electronics then measure the shape of each light pulse and rejects fast-risetime events which show that a charged particle has passed through the outside scintillator. This detector is called a *phoswich*, short for 'phosphor sandwich'. Scintillation counters have been the workhorses of balloon-based high-energy X-ray astronomy. At altitudes of more than 40 km, observations have been made in the energy range 20–200 keV.

3.1.4 Channel electron multiplier and micro-channel plate

The channel electron multiplier is a small-diameter glass tube which has been treated to enhance secondary emission properties. The pore

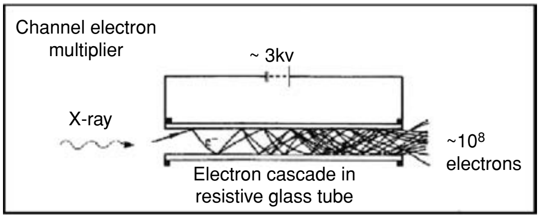

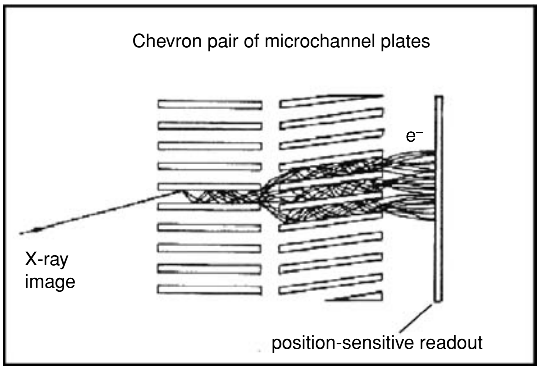

Fig 3.3 The micro-channel plate is a bundle of thousands of small glass tubes, each of which gives a large gain in the signal. A pair of plate assemblies prevents light from directly reaching the detector, and an image is transfered with high gain from the front surface to the detector.

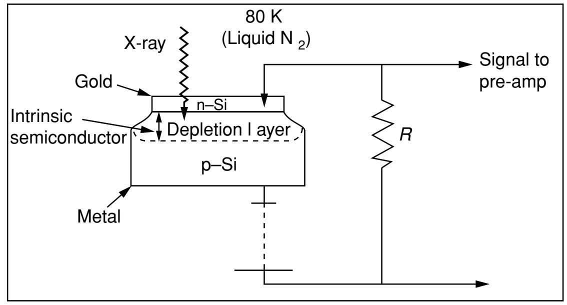

Fig 3.4 Diagram of the Einstein solid state spectrometer (SSS). The SSS was a reverse-biased junction that created a depletion layer as its detecting volume. An interacting X-ray produced ion pairs in this volume as in a proportional counter gas, but much more easily, and there was no avalanche. To reduce thermal noise, the whole system was cooled to 80 K, and a low noise amplifier was required.

diameter is $\approx 10\mu$. A high voltage is applied along the length of the tube. A photon striking the inside of the negative end ejects low-energy electrons which are accelerated down the tube. As they progress, they strike the wall and liberate more electrons. The original electrons become a cascade of as much as 10^8 electrons at the positive end. The negative end, or photocathode, is coated with CsI to improve the efficiency of X-ray photoelectron emission.

A micro-channel plate (or MCP) is a position-sensitive detector useful for recording images. It is simply a very large number of such tubes fused together by means of glass fibre technology. They have extensive military applications and are perhaps best known for their use in night-vision binoculars. A typical MCP of 25 mm diameter might have 3 million individual micro-channels, each 20 μm across. It is capable of producing a gain of about 10^4 (i.e. a single electron entering a micro-channel will be amplified to yield 10^4 electrons at the other end, as shown in Fig. 3.3). The spacing of the channels is so small that the incident image is reproduced as an electron image which can be recorded by a variety of techniques. The Einstein and ROSAT high-resolution imager (HRI) detectors and the Chandra high-resolution camera (HRC) utilised micro-channel plates.

3.1.5 Solid state detector and charge-coupled devices

The solid state spectrometer (SSS) was first flown on Einstein and is shown schematically in Fig. 3.4. The incoming X-ray ionises atoms of material in the detector, but because the material is solid silicon and the applied voltage is low, there is no avalanche. The SSS collects the free electrons and measures the charge directly. This worked because the detector was solid state and was cooled to very low temperatures (80 K or $-193\,^{\circ}$C) so that thermal noise was greatly reduced. Because each X-ray which deposited energy in the detector initially generated many more ion pairs than in the gas of a proportional counter, the resolution of the SSS was about three times better, yet with virtually no loss of efficiency.

Technology has advanced to the point where the SSS can be made much smaller and can be placed in arrays of $\sim 10^6$ detectors. These devices, the charge-coupled devices (CCDs), have been used in ground-based optical astronomy for more than 2 decades now, with revolutionary results. Their substantial gain in efficiency over previous devices has been directly responsible for many of the important discoveries of observational astronomy

Fig 3.5 The Chandra ACIS detector. The 2 × 2 ACIS-I and the 1 × 6 ACIS-S chip arrays are visible at the top (NASA/CXC 2010).

since ∼1980. The Chandra CCD is shown in Fig. 3.5. In this device, each chip of 1024 × 1024 pixels is 2.5 cm wide. The device is operated like a camera, and data are recorded during an interval of 3.2s. If an X-ray is absorbed in a pixel, a charge proportional to the photon energy is deposited there. At the end of the recording interval, the device is read out one row at a time by circuitry at one edge of the chip. After the first row is read out, charge in all pixels is shifted down one row and the second row is read out. This charge-transfer *clocking* process takes only 0.04 s to read all 1024 rows.

During normal operation, almost all pixels contain no charge, and only a few have charge deposited by a single X-ray. If the source is bright and the focus sharp, there can be two or more interactions in a single pixel during the 3.2-s recording interval. This charge is recorded as a single event having the summed energy of the interacting photons. This is *pileup*, a distortion of the spectrum which becomes worrying at count rates above ∼0.01 counts pix^{-1} s^{-1}. A very bright source will deposit many X-rays in a few central pixels during each recording cycle, and the charge can be so large that the event is rejected. An image of a very bright point source appears as a bright halo with a hole at the centre. Also, events are recorded during readout as the rows are clocked through the source location. This is the *charge transfer streak* or *CT streak*, which appears as a number of bright columns radiating from the source. Figures 3.6, 5.7 and 5.10 show bright CT streaks.

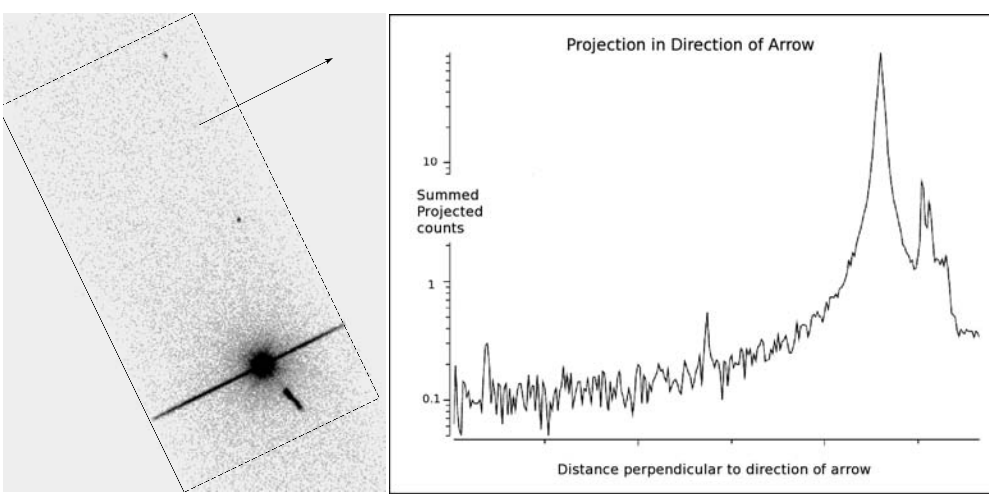

Fig 3.6 (left) A 40-ks Chandra ACIS image of the quasar 3C 273. The field covers 1.3′ × 2.6′ of the sky. The quasar itself is a bright point source, overexposed in this presentation and with CT streak. There is a jet pointed southwest, separated from the quasar and with internal structure. The grey scale has been adjusted to show the broad, outer part of the mirror PSF. The width of the CT streak shows the size of the core of the PSF. (right) The image has been projected in the direction of the arrow, and the graph gives number of counts (log scale) in each column and shows structure within the jet. The core of the image is distorted by pileup and the CT streak. Note that the two faint sources are more easily visible in the image than in the projection.

3.1.6 Calorimeter

A remarkable and completely new device was developed and flown on the Suzaku mission in 2005. This was the quantum calorimeter, in which individual X-ray photons are absorbed by a crystal which is maintained at a temperature very close to absolute zero ($\leq$0.1 K). The energy of the X-ray causes the temperature of the crystal to increase, and this is measured. The higher the energy of the photon, the greater the temperature increase; hence the device is a spectrometer. An energy resolution of 6 eV ($\sim$20 times better than the SSS!) was achieved (Kelley *et al.*, 2007).

Unfortunately, the Suzaku refrigerator failed, and no astronomy data were obtained with this detector. The method does show great promise, however, and calorimeters are planned for future missions. Much new technology is required. The temperature rise from an event is minute, and a very sensitive thermometer is needed. Some designs use a superconducting layer in thermal contact with the absorber to measure the temperature rise. Maintaining a low temperature for a long time is always a challenge. Furthermore, in a large array, a low temperature cannot be maintained if a wire connects each pixel to the warm environment. The rate of heat transfer must be minimised by using a pixel readout multiplexer built into the cold detector. As Table 3.1 shows, the gain in resolving power over the CCD is considerable, and an extensive development effort will be well worthwhile.

Table 3.1 Spectral resolving power of detectors and dispersive spectrometers.

	Energy (keV)			
	0.5	1	6	20
Proportional counter RXTE	–	–	5.5	10
Imaging proportional counter ROSAT	2	3	–	–
CCD(ACIS) Chandra	5	11	40	–
CCD(MOS) XMM	8	14	38	–
Calorimeter	80	160	1000	
LETG Chandra	631	314	50	–
HETG/HEG Chandra	–	1351	225	–
RGS XMM	466	156	–	–

3.1.7 Detection of polarisation

Polarisation measurements would be extremely valuable in the study of almost all types of cosmic sources. For example, scattering produces polarisation, and so an observation of an accretion disc corona might reveal how the material is distributed (see Chapter 11). Because emission in a magnetic field will produce polarised X-rays, we can learn details about the emission from pulsar-wind nebulae and from neutron star surfaces (see Chapter 9).

However, determining the level of X-ray polarisation is technically challenging, and there has been little progress through the history of X-ray astronomy. The first detectors utilised Thompson or Bragg scattering, in which the direction of the electric vector is preserved. Because this direction is always perpendicular to the direction of propagation, scattering of a linearly polarised beam is not isotropic. In particular, if the scattering angle is 90°, there is no scattering in the direction of the incident electric vector. This anisotropic scattering was the basis for the first detectors used to search for polarised X-rays from cosmic sources. These detectors comprised a scatterer and counters to register X-rays scattered at angles of $\approx$90°. When these detectors were rotated around the incident beam direction, the dependence of count rate on rotation angle was a measure of beam polarisation.

Because absorption is minimum in low-Z elements, the first rocket payload utilised Thompson scattering from Li blocks. A more sensitive crystalline-graphite Bragg instrument on the satellite OSO-8 actually managed to measure the polarisation of the Crab Nebula and set limits of a few per cent on polarisation from several bright accretion-powered binaries. To date, the only polarisation measure of X-rays from an extra-solar source is that of the Crab Nebula, 19 $\pm$ 2 per cent, by Weisskopf *et al.* (1978).

New proportional counters are under development which promise a great gain in the efficiency of polarisation measurements. These incorporate internal structure which gives signals dependent

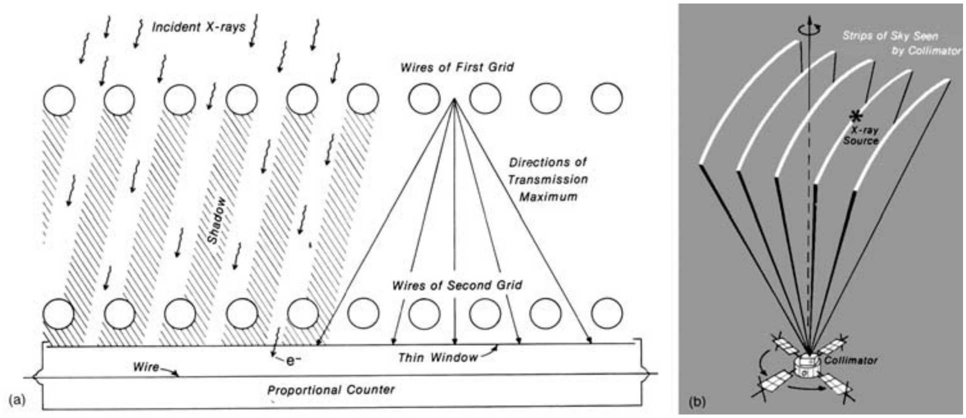

Fig 3.7 The modulation collimator. (a) Two separated wire grids define a set of bands on the sky through which X-rays can be seen. If the spacecraft rotates, a point source in the field of view will cross these bands and produce a modulated count rate as a function of time. (b) If the rotation axis is parallel to the pointing direction, the response pattern depends on where the source is within the overall field of view of the collimator, and the location of the source can be determined typically to $1'$.

on the direction of photoelectrons that are produced by X-ray interactions within the detector. Because photoelectrons are emitted in a direction approximately parallel to the electric vector of the incident X-ray, this directly measures polarisation. Two new designs are the gas pixel polarimeter (Bellazzini *et al.*, 2006) and the time projection chamber (Hill *et al.*, 2007).

3.2 Location of cosmic X-ray sources

3.2.1 Slat collimator

Early observations used detectors with simple slat or *honeycomb* collimators which restricted the detector field of view. One narrow and one broad dimension combined with a spinning spacecraft produced a scan of a strip of sky. Width of the strip was determined by the broad dimension. The narrow dimension produced a one-dimensional position of the source along the strip. A subsequent scan with different orientation would enable a two-dimensional location of sources on the sky with positional accuracy dependent on the collimator dimension and source strength. See figures in Chapter 1, e.g. Figs. 1.5 and 1.6

3.2.2 Scanning modulation collimator

In this scheme, a slat-collimated detector viewed the sky through a one-dimensional wire grid. As the detector scanned across the source, the signal was modulated by the shadow pattern of the grid, as shown in Fig. 3.7. The area of the detector was somewhat sacrificed to achieve this fine-scale modulation of the signal, which improved the location accuracy significantly. It essentially allowed the information about the spatial distribution of sources on the sky to be transformed into a temporal signal which could be easily registered by early X-ray astronomy detectors. The modulation collimator was used on a rocket flight in 1966 to locate Sco X-1 well enough to identify the optical counterpart (Gursky *et al.*, 1966). Arcminute locations of most of the bright sources were then obtained by modulation collimators on board the satellites SAS-3 and HEAO-1. Both linear and rotational scans were used.

3.2.3 Coded mask

An extension of the modulation collimator technique was developed in the 1970s, in which a *coded mask* is placed in front of a detector, making it possible to view a moderately large region of sky with a single pointing and with moderate spatial resolution. It is not an imaging device but more a pinhole camera with many pinholes. A sheet of absorbing material with a random pattern of openings casts a shadow on a position-sensitive detector, as illustrated in Colour Plate 5. The pattern in the detector is correlated with the known pattern in the mask, and the two patterns match in only the direction to the source. If the mask is made larger than the detector, coverage of the field is uniform, except at the edges. Coded masks have been used for 'imaging' of high-energy X-rays and γ rays because they cannot be focussed in the same manner as low-energy X-rays (see Section 3.2.5). The data in Fig. 13.11 were obtained with an early-coded mask. Colour Plate 5 shows a schematic of a large coded detector on the INTEGRAL spacecraft.

3.2.4 Lunar occultation

A source can be accurately located in one dimension by observing it pass behind the limb of the Moon and exploiting our precise knowledge of the Moon's position in the sky. As in the earlier sections, this converts temporal into spatial information. The orbital motion of the Moon is $\approx 0.5'' \text{ s}^{-1}$, and the resulting precision of the X-ray source location will depend on its strength. For an isolated source a rate of ≈ 10 counts s^{-1} is needed for an accuracy of $1''$. The motion of the spacecraft must also be taken into account, so considerable preparation is needed to observe occultations. Figure 3.8 shows a lunar occultation of the Crab Nebula, a very bright X-ray source, observed with a large rocket-borne proportional counter. Colour Plate 9 shows an occultation of a galactic source observed by ROSAT.

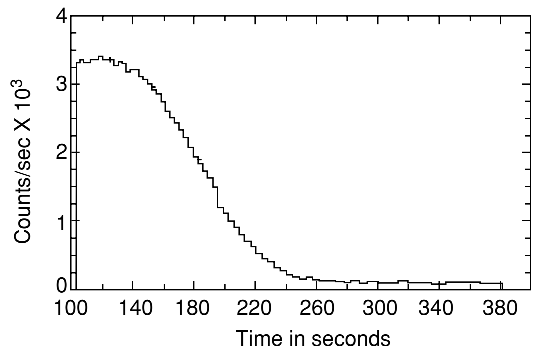

Fig 3.8 Counting rate of a rocket-borne X-ray detector during a lunar occultation of the Crab Nebula. As the Moon passed in front of the nebula, the source within the Crab was gradually occulted over 120 s of time, showing that it is $\approx 2'$ in extent. The neutron star within the Crab, however, accounts for 5 per cent of the X-ray flux and is a point source. When the neutron star passed behind the lunar limb at 195 s, a sudden drop in count rate was observed (from Palmieri *et al.*, 1975).

3.2.5 Mirrors and telescopes

X-rays will reflect from smooth surfaces if the incidence angle is small. If the surface is truly smooth and the incidence angle $<1^\circ$, reflection efficiency is close to 1. For a given energy, as the angle is increased, efficiency stays high until a critical angle, θ_c, after which reflection efficiency drops rapidly (as shown in Fig. 3.9 for some materials used in current-generation X-ray mirrors). For photon energy E and electron density ρ, then $\theta_c = c\sqrt{\rho}/E$. In a telescope, the angle is fixed. Reflection efficiency is high up to a point, then falls rapidly for energies such that the reflection angle is greater than the critical angle. Thus telescope mirrors have a high energy cut-off, and dense (high-Z) materials have the largest critical angles. At 0.75° X-rays are reflected from polished quartz up to ≈ 2 keV, from polished nickel up to ≈ 4 keV and from polished gold up to ≈ 6 keV. At 0.5° the Ni and Au cutoffs are raised to 6 and 9 keV, respectively.

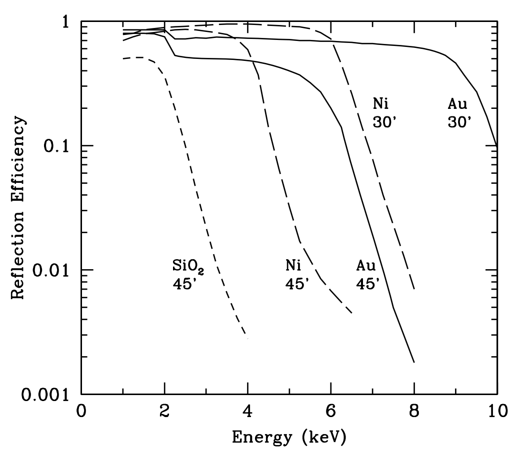

Fig 3.9 Efficiency of X-ray reflection from polished surfaces of quartz (short-dashed line), nickel (long-dashed line) and gold (solid line). Incidence angles are 0.5° (30 arcmin) and 0.75° (45 arcmin). Reflectivity is highest at low energies and small angles (from Seward, 1977).

A parabolic mirror surface can be made or approximated which, with one reflection, will